Prior image-constrained ℓ_1-norm-based reconstruction method for effective usage of structural information in diffuse optical tomography

Calvin B. Shaw and Phaneendra K. Yalavarthy*

Supercomputer Education and Research Centre, Indian Institute of Science, Bangalore 560 012, India
**Corresponding author: phani@serc.iisc.in*

Received July 20, 2012; accepted September 12, 2012;
posted September 14, 2012 (Doc. ID 172959); published October 15, 2012

A novel approach that can more effectively use the structural information provided by the traditional imaging modalities in multimodal diffuse optical tomographic imaging is introduced. This approach is based on a prior image-constrained-ℓ_1 minimization scheme and has been motivated by the recent progress in the sparse image reconstruction techniques. It is shown that the proposed framework is more effective in terms of localizing the tumor region and recovering the optical property values both in numerical and gelatin phantom cases compared to the traditional methods that use structural information. © 2012 Optical Society of America

OCIS codes: 170.0170, 170.3010, 170.6960, 100.3190, 170.5280, 110.4190.

Diffuse optical tomography in combination with the traditional imaging modalities, such as Magnetic Resonance Imaging (MRI), computed tomography (CT), and ultrasound, has been shown to have a distinct advantage when compared to the diagnostic information provided by each one separately [1,2]. Usage of structural information provided by the traditional imaging modalities to guide and improve the diffuse optical image characteristics has been an active area of research.

Two prominent reconstruction methods that use structural information are *soft-priors*, which uses the structural information in the regularization, and *hard-priors*, which constrains the number of optical parameters to be reconstructed to be equal to the number of distinct tissue types determined by the traditional imaging modalities [2]. In scenarios where the traditional imaging modalities are known to give false positives in cancer imaging, the *hard-priors* based approach becomes prohibitive to be used, as its solutions are biased toward structural information [1,2]. The approach that is commonly deployed in these cases is *soft-priors*, which can provide more flexibility in the usage of structural information [1,2].

The *soft-priors* based approach employs traditional ℓ_2-norm-based regularization to stabilize the solution [2], resulting in smoothened reconstructed image features as it constrains the solution to have any sharp changes [3]. To overcome this limitation, in this Letter, we propose a prior image-constrained ℓ_1-norm-based (PIC-ℓ_1) regularization for effective usage of structural information.

This work has been motivated by the recent studies of the prior image-constrained compressed sensing approach for perfusion CT, which was proven to be effective in providing high signal to noise ratio (SNR) images with limited projection data [4]. In our case, the prior image refers to the structural information provided by the traditional imaging modality without the tumor information. For example, in the case of breast imaging this could be, knowing only the adipose/fatty and fibro-glandular tissue region information. The performance of PIC-ℓ_1 is compared with the traditional methods for numerical breast phantom and experimental gelatin phantom cases to show the effectiveness of the proposed method. The discussion in here is limited to the two-dimensional continuous-wave (CW) case as the emphasis is on showing the effectiveness of the proposed method without the tumor information in the prior image.

The near-infrared (NIR) light propagation in thick tissues, such as breast, is modeled using the diffusion equation (DE), and for the CW case [5] it is given by

$$-\nabla . D(r)\nabla\Phi(r) + \mu_a(r)\Phi(r) = Q_o(r), \tag{1}$$

where $\Phi(r)$ is the photon fluence at a given position r and $Q_o(r)$ is the isotropic light source at position r. $\mu_a(r)$ denotes the spatially varying optical absorption coefficient (parameter to be estimated) with units of mm^{-1} and $D(r)$ is the optical diffusion coefficient (assumed to be known) and is given by $1/[3(\mu_a + \mu_s')]$ with μ_s' representing the reduced scattering coefficient. Typically the finite-element-based method is deployed to solve DE along with a type-III boundary condition that accounts for the refractive-index mismatch [5]. The sampled version of $\Phi(r)$ at detector locations forms the modeled data ($G(\mu_a)$).

The inverse problem of estimating μ_a for the *soft-priors* case is posed as a minimization problem with the objective function [1,2] as

$$\Omega_1 = \frac{1}{2}\|y - G(\mu_a)\|^2 + \frac{\lambda_1}{2}\|\mathbf{L}(\mu_a - \mu_{a0})\|^2 \tag{2}$$

with y representing the experimental data and μ_{a0} as the prior estimate of the μ_a using a calibration procedure. The regularization parameter here is represented by $\lambda_1(>0)$ with $\mathbf{L}$ denoting the Laplacian matrix, which is a smoothing operator that contains the region information with entries as 1 on the diagonal, $\mathbf{L}_{ij} = -1/n$ at the off-diagonal entries when i and j belong to the same region containing n number of nodes, and 0 elsewhere [2]. The iterative update equation for minimizing Eq. (2) is given by [2]

$$\Delta\mu_a = (\mathbf{J}^\mathbf{T}\mathbf{J} + \lambda_1\mathbf{L}^\mathbf{T}\mathbf{L})^{-1}\mathbf{J}^\mathbf{T}\delta \tag{3}$$

with $\delta = y - G(\mu_a)$ as the data-model misfit and $\mathbf{J}$ representing the Jacobian ($= dG(\mu_a)/d\mu_a$). Note that when $\mathbf{L}$ is equal to the identity matrix, the resulting reconstruction procedure is an ℓ_2-norm-based standard reconstruction procedure without any prior information.

For the proposed PIC-ℓ_1 reconstruction method, the objective or cost function [4] for the update $\Delta\mu_a$ can be written as

$$\Omega = \alpha\|\psi_1(\Delta\mu_a - \mu_a^{\mathrm{pr}})\|_1 + (1-\alpha)\|\psi_2(\Delta\mu_a)\|_1 \quad \text{s.t. } \mathbf{J}\Delta\mu_a = \delta, \tag{4}$$

where $\Delta\mu_a$ is the unknown (with respect to which above equation is minimized), μ_a^{pr} is the prior image with structural priors, and $\psi_{1,2}$ are two sparsifying transformations [here, discrete cosine transform (DCT)]. The parameter α ($0 \le \alpha \le 1$) dictates the dependency on the prior image, with α being 0 representing the conventional ℓ_1-norm-based algorithm without any usage of prior information and α being 1, denoting the correction to the prior image [4]. In this Letter, $\alpha = 0.8$ was used in all cases. Equivalently the minimization given in Eq. (4) could be written as (also known as the unconstrained variant [4])

$$\Omega_2 = \alpha\|\psi_1(\Delta\mu_a - \mu_a^{\mathrm{pr}})\|_1 + (1-\alpha)\|\psi_2(\Delta\mu_a)\|_1 + \frac{\lambda_2}{2}\|\mathbf{J}\Delta\mu_a - \delta\|_2^2, \tag{5}$$

where λ_2 is a regularization parameter (>0). Equation (5) is minimized using a simple Newton's method, requiring the computation of the gradient and Hessian of the cost function.

The ℓ_1-norm is the sum of absolute values and is not a smooth function, making the gradient or the Hessian of the cost function not well defined for all values of $\Delta\mu_a$. Instead, we approximate the ℓ_1-norm with a smooth function by using the relation $\|\mu_a\|_1 \approx \sqrt{\Delta\mu_a^*\Delta\mu_a + \beta}$, where β is a smoothing parameter [6], which is typically chosen as a small value (here, 1e-7). With this approximation, one can construct a diagonal matrix $\Lambda|_{\Delta\mu_a}$ with entries defined as $\Lambda_i|_{\Delta}\mu_a = \sqrt{(\psi\Delta\mu_a)_i^*(\psi\Delta\mu_a)_i + \beta}$ [6], where $\psi = \psi_1 = \psi_2$ (DCT). Differentiating Eq. (5) with respect to the unknown ($\Delta\mu_a$) yields

$$\nabla\Omega_2|_{\Delta\mu_a} = \alpha\psi^T(\Lambda|_{\Delta\mu_a - \mu_a^{\mathrm{pr}}})^{-1}\psi(\Delta\mu_a - \mu_a^{\mathrm{pr}}) + (1-\alpha)\psi^T(\Lambda|_{\Delta\mu_a})^{-1}\psi(\Delta\mu_a) + \lambda_2 J^T(\mathbf{J}\Delta\mu_a - \delta). \tag{6}$$

Now, the update equation that minimizes Eq. (5) becomes

$$\Delta\mu_a^{t+1} = \Delta\mu_a^t - \mathbf{H}^{-1}|_{\Delta\mu_a^t}\nabla\Omega_2|_{\Delta\mu_a^t}. \tag{7}$$

The t in here represents the inner iteration number and the (linear) Hessian approximation ($\mathbf{H}$) is given as [4]

$$\mathbf{H}|_{\Delta\mu_a} = \alpha\psi^T(\Lambda|_{\Delta\mu_a - \mu_a^{\mathrm{pr}}})^{-1}\psi + (1-\alpha)\psi^T(\Lambda|_{\Delta\mu_a})^{-1}\psi + \lambda_2\mathbf{J}^{\mathbf{T}}\mathbf{J}. \tag{8}$$

Similar to earlier case [Eq. (3)], the computed $\Delta\mu_a$ is added to the current μ_a for recomputation of $\mathbf{J}$ and δ.

Initially, a numerical experiment with derived structures from human breast in a typical MRI-NIR exam is conducted. The target μ_a distribution is given in the top-left corner of Fig. 1(a). There are three types of tissue regions, namely fatty ($\mu_a = 0.01$ mm^{-1} and $\mu_s' = 1.0$ mm^{-1}; region number: 0), fibro-glandular ($\mu_a = 0.015$ mm^{-1} and $\mu_s' = 1.0$ mm^{-1}; region number: 1), and tumor ($\mu_a = 0.02$ mm^{-1} and $\mu_s' = 1.0$ mm^{-1}; region number: 2). The data acquisition set up had 16 light collection/delivery fibers that were arranged in an equispaced fashion; when one acts as a source, others become detectors, resulting in total 240 intensity measurements. A fine mesh consisting of 4876 nodes (corresponding to 9567 triangular elements) is used for generating experimental data, and a coarser mesh with 1969 nodes

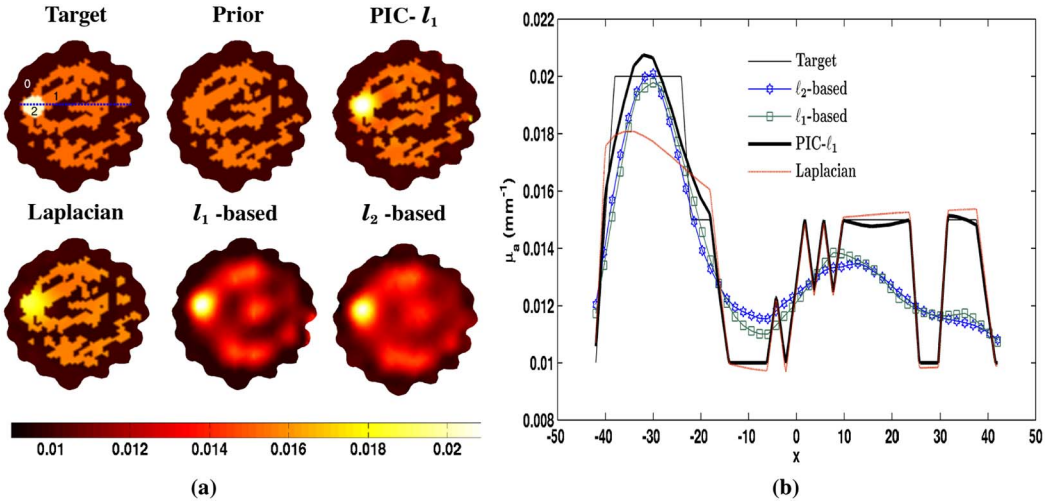

Fig. 1. (Color online) (a) Reconstructed μ_a distributions using reconstruction methods described in this Letter with numerically generated 1% noisy data using the target image (top-left). (b) The one-dimensional cross-sectional plot along the dashed line given in the target image for the reconstructed images in (a). The regularization parameters that were used are 80, 40, 20, and 50 for PIC-ℓ_1, Laplacian, ℓ_1-norm-based, and ℓ_2-norm-based reconstruction methods, respectively.

(corresponding to 3753 triangular elements) was used in the reconstruction. The numerically generated data using fine mesh was added with 1% uniformly distributed Gaussian noise to mimic the experimental case. The optical properties of the fatty region were used as homogenous initial guesses to the reconstruction procedures described earlier. The iterative procedure was stopped once $\|\delta\|^2$ did not improve by more than 2% when compared to the previous iteration.

Totally four reconstruction methods were considered for reconstruction of the numerical data, namely proposed PIC-ℓ_1 [Eq. (7)], Laplacian-based soft-priors [Eq. (3)], ℓ_1-norm-based method [Eq. (7), with $\alpha = 0$, no priors], and ℓ_2-norm-based method [Eq. (3) with $\mathbf{L} = \mathbf{I}$, no priors]. The reconstructed μ_a images are given in Fig. 1(a), where corresponding to each image the reconstruction method used is given on top of each distribution. The regularization parameter values that were used are given in the caption of Fig. 1, as they provided the best possible solutions. Note that the prior image (μ_a^{pr}) is computed for PIC-ℓ_1 using the *hard-priors* approach [2] with only fatty and fibro-glandular regions, and the resulting image is also given in Fig. 1(a).

As seen from Fig. 1, the performance of ℓ_1- and ℓ_2-based reconstruction methods without structural information has been poor (especially in spatial resolution characteristics) compared to PIC-ℓ_1 and Laplacian based *soft-priors* method. Among the later two, the performance of PIC-ℓ_1 was higher in terms of localizing the tumor and providing better contrast recovery [see Fig. 1(b)].

Next, a gelatin cylindrical phantom (height 25 mm and diameter 86 mm) that mimics the breast tissue was fabricated using mixtures of water (80%), gelatin (20%), India ink for absorption, and TiO_2 for scattering [7]. The two-dimensional cross section showing the distribution of μ_a is given in the top-left corner of Fig. 2(a). The region labeled as '0' has the optical properties of $\mu_a = 0.0065\ \mathrm{mm}^{-1}$ and $\mu_s' = 0.65\ \mathrm{mm}^{-1}$ (mimicking fatty layer) and had a thickness of 10 mm. The fibro-glandular layer was labeled as region '1' had a diameter of 76 mm with optical properties of $\mu_a = 0.01\ \mathrm{mm}^{-1}$ and $\mu_s' = 1.0\ \mathrm{mm}^{-1}$. The tumor region labeled as '2' had a diameter of 16 mm with optical properties of $\mu_a = 0.02\ \mathrm{mm}^{-1}$ and $\mu_s' = 1.2\ \mathrm{mm}^{-1}$. A mesh having 1785 nodes corresponding to 3418 linear triangular elements was used for the reconstruction. The data was collected in the Dartmouth-NIR system at 785 nm. Similar to the earlier case, it was assumed that only μ_a is unknown and the prior image (considering only regions: 0 and 1) is computed using *hard-priors*. Here, only PIC-ℓ_1 and Laplacian based *soft-priors* reconstruction methods were used as they were proven to be effective compared to others

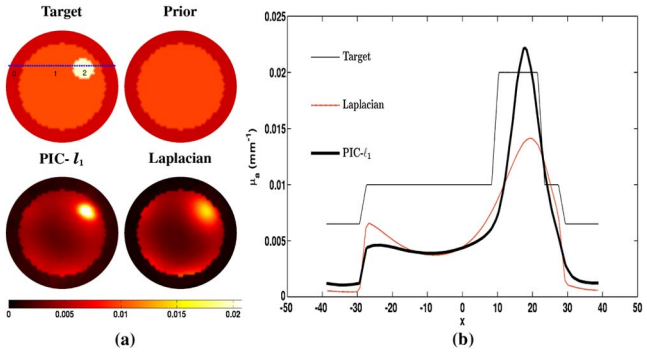

Fig. 2. (Color online) Similar effort as Fig. 1 for the case of gelatin phantom data, except only PIC-ℓ_1 and Laplacian based reconstruction methods were used. The corresponding regularization parameters that were used are 10 and 20.

in the numerical experimental case. The reconstruction results are given in Fig. 2. It is also evident from this case that the localization of tumor region is better with the PIC-ℓ_1 reconstruction method and the recovered μ_a values for the tumor region are more close to target values.

In conclusion, we have presented a novel approach for usage of structural prior information in a diffuse optical image reconstruction framework and proven that the proposed method is more effective in localizing the tumor and providing better contrast recovery compared to its counterparts.

The authors gratefully acknowledge the Dartmouth NIR imaging group for providing necessary patient mesh and phantom data that were used in this work. This work is supported by the Department of Atomic Energy Young Scientist Research Award (No 2010/20/34/6/BRNS)

References

1. C. M. Carpenter, B. W. Pogue, S. Jiang, H. Dehghani, X. Wang, K. D. Paulsen, W. A. Wells, J. Forero, C. Kogel, J. B. Weaver, S. P. Poplack, and P. A. Kaufman, Opt Lett. **8**, 933 (2007).
2. P. K. Yalavarthy, B. W. Pogue, H. Dehghani, C. M. Carpenter, S. Jiang, and K. D. Paulsen, Opt. Express **15**, 8043 (2007).
3. C. B. Shaw and P. K. Yalavarthy, J. Biomed. Opt. **17**, 086009 (2012).
4. J. C. Ramirez-Giraldo, J. Trzasko, S. Leng, L. Yu, A. Manduca, and C. H. McCollough, Med. Phys. **38**, 2157 (2011).
5. H. Dehghani, S. Srinivasan, B. W. Pogue, and A. Gibson, Phil. Trans. R. Soc. A **367**, 3073 (2009).
6. M. Lustig, D. Donoho, and J. M. Pauly, Magn. Reson Med. **6**, 1182 (2007).
7. B. W. Pogue and M. Patterson, J. Biomed. Opt. **11**, 041102 (2006).